Microvascular Research 101 (2015) 62–71

Contents lists available at ScienceDirect

Microvascular Research

journal homepage: www.elsevier.com/locate/ymvre

Numerical simulation of the tumor interstitial fluid transport: Consideration of drug delivery mechanism

Mohammad Charjouei Moghadam, Amin Deyranlou, Alireza Sharifi, Hamid Niazmand *

Department of Mechanical Engineering, Ferdowsi University of Mashhad, Mashhad, Iran
Research Center for Biomedical Engineering, Ferdowsi University of Mashhad, Mashhad, Iran

ARTICLE INFO

Article history:
Accepted 13 June 2015
Available online 27 June 2015

Keywords:
Computational modeling
Tumor
Surrounding normal tissue
Interstitial fluid transport
Drug delivery

ABSTRACT

The interstitial fluid transport plays an important role in terms of its effect on the delivery of therapeutic agents to the cancerous organs. In this study, a comprehensive numerical simulation of the interstitial fluid transport establishing 3D models of tumor and normal tissue is accomplished. Different shapes of solid tumors and their surrounding normal tissues are selected, by employing the porous media model and incorporating Darcy's model and Starling's law. Besides, effects of the tumor radius, normal tissue size, tissue hydraulic conductivity and necrotic core are investigated on the interstitial fluid pressure (IFP) and interstitial fluid velocity (IFV). Generally, results suggest that the configurations of the tumor and surrounding normal tissue affect IFP and IFV distributions inside the interstitium, which are much more pronounced for various configuration of the tumor. Furthermore, findings demonstrate that larger tumors are more prone for producing elevated IFP comparing with the smaller ones and impress both IFP and IFV dramatically. Nevertheless, normal tissue size has less impact on IFP and IFV, until its volume ratio to the tumor remains greater than unity; conversely, for the values lower than unity the variations become more significant. Finally, existence of necrotic core and its location in the tumor interstitium alters IFP and IFV patterns and increases IFV, considerably.

Introduction

Cancer, an initially asymptomatic disease, befalls as a consequence of abnormal cell growth, which is potentially disposed to disperse through other organs and is regarded as the second leading cause of human's mortality (Siegel et al., 2013). Smoking, obesity, lack of physical activity and poor diets are among major causes of the disease occurrence. In cancerous tumors, a large milieu of cancer cells form a mass of tumor, which are usually feeding from nutritional material through angiogenic vasculature (Jain, 2005). Therefore, employing ample medical techniques to impede tumor activity from growth and dispersion throughout the body arouses many explorations in this regard.

Among various cancer treatment methods, tumor excising is the most intrusive one. Nevertheless, thorough eradication of malignant tumors through surgical removal seems a hard-reaching task. Thus, post-operative measures such as chemotherapy, radiotherapy and combined methods play a substantial role in conflict with tumor re-growth and even its multiplication (Tan et al., 2003). In these conventional techniques, an anticancer agent is injected intravenously through systemic administration in order to either demoralize or halt tumor growth. However, drug toxicity of healthy organs and non-uniform distribution of extravasated blood around a tumor impedes successful drug delivery to the cancerous tissues (Jain and Baxter, 1988; Jain, 1988). Indeed inadequate proliferation of tumor sites by therapeutic agents lowers efficiency of target therapy in the pertinent maladies. Studies have demonstrated that in addition to heterogeneous blood supply, non-uniform binding of antigens and antibodies and interstitial blockage of drug transport to a tumor, elevated interstitial pressure inside the tumor is a main non-immunological factor, which is contributed to poor drug delivery (Jain, 1988; Baxter and Jain, 1989). In the following, a brief review of most prominent work in this regard is presented.

Jain (1988) implemented a review on tumorous tissue morphology and determining factors on blood flow in the vascular network. Baxter and Jain (1989) established a theoretical framework to examine the role of interstitial fluid pressure (IFP) on tumor drug delivery. They demonstrated that lack of lymphatic drainage vessels inside the tumor increases IFP, which influences on drug delivery especially from two senses, i.e., reduction in motive force for transcapillary exchange of drug and growing convective efflux of interstitial fluid toward the tumor rim. Later, similar conclusions were made by Boucher et al. (1990) through an experimentation on two rat tissue-isolated tumors. In more developed studies Baxter and Jain (1990,1991) incorporated effects of lymphatic drainage vessels, heterogeneous perfusion of

* Corresponding author at: Department of Mechanical Engineering, Ferdowsi University of Mashhad, Mashhad, Iran.
E-mail addresses: mcharjoie@gmail.com (M.C. Moghadam), deyranlou.amin@gamil.com (A. Deyranlou), sharifialireza@yahoo.com (A. Sharifi), niazmand@um.ac.ir (H. Niazmand).

http://dx.doi.org/10.1016/j.mvr.2015.06.007
0026-2862/

tumor and extravascular binding to provide more realistic framework of macromolecular transport in tumors. In a new effort Netti et al. (1995) demonstrated dependency of IFP to variations of microvascular pressure and tumor blood flow through analytical solution and ex-vivo experimentation.

Examining various antineoplastic agents and determinant, especially IFP effects for obtaining adequate drug delivery via target therapy through tumorous sites, sparked new efforts to explore idealized and actual specific-patient tumorous tissues by extending formulations for two (2D) and three-dimensional (3D) coordinate systems. Wang et al. (1999) studied BCNU delivery to the 3D reconstructed MRI images of brain tumors and estimated anticancer concentrations through in. Similarly Goh et al. (2001) developed 2D simulation for investigating transport of doxorubicin to the hepatic tumor (hepatoma) both spatially and temporally inside the tumor and its surrounding normal tissues. Moreover, many relevant studies have been carried out such as those implemented by Pozrikidis and Farrow (2003), Teo et al. (2005), J. Zhao et al. (2007), and Linninger et al. (2008). More additionally invoking 3D models, Wang and Li (1998), Tan et al. (2003) and Teo et al. (2005) studied drug delivery through systematic administration and polymer-based release, numerically.

Other important studies in the scope of cancerous tumors can refer to those accomplished for better understanding of angiogenesis. In the angiogenesis, tangled networks of microvasculature are formed throughout the tumor for nourishment of cancer cells. Among most important work in this scope one can refer to Anderson and Chaplain (1998), Stéphanou et al. (2006), Harrington et al. (2007), G. Zhao et al. (2007), Cai et al. (2011), Soltani and Chen (2013), Yifat and Gannot (2014) and Sefidgar et al. (2015). Despite the number of numerical investigations that have been accomplished on the tumor angiogenesis, however fewer studies are focused on the tumor interstitial pressure distribution, which may be influenced by either tissues configurations or their physiological properties. El-Kareh and Secomb (1995) invoked theoretical framework in order to mainly investigate effects of microvessels hydraulic conductivity on macromolecular transport to the tumor. J. Zhao et al. (2007) and Pishko et al. (2011) simulated drug delivery through specific tumorous tissue, which had been obtained from MRI technique and examined effects of heterogeneous vasculature and porosity. Recently, Soltani and Chen (2011,2012) and Sefidgar et al. (2014) have studied effects of various tumor configurations and transport properties on drug distribution by incorporating fluid and concentration equations.

In summary, abovementioned studies have unfurled new insights for better understanding about tumor pathology; however, there are several aspects that have not been dug carefully. To the best of authors' knowledge, previous investigations neglected effects of simultaneous variations of tumor and its surrounding normal tissue configurations, the issue that seems crucial in drug delivery.

Therefore, the main object of the current study is examining effects of the geometrical specifications of both the tumor and its surrounding normal tissue on IFP and IFV, through extensive numerical simulations on 3D models. Tumor radius, the volume ratio of the normal tissue to the tumor and their configurations are among those specifications, which are explored thoroughly. The porous media model is adopted for the simulation incorporating the fluid source and lymphatic drainage terms to account for the fluid exchange between the interstitial space and blood or lymph vessels. Furthermore, effects of the interstitium hydraulic conductivity are investigated. Finally, in the last section IFP and IFV distributions are studied for heterogeneous tumor by including necrosis inside different locations of the interstitium, the subject that is considered less attention.

Mathematical modeling

Inside the body, tissues mainly consist of the vasculature network, the interstitial space and the cellular space. The cellular space where the cancer cells are located inside a tumor includes other cells such as pericytes, macrophage and fibroblast (Baxter and Jain, 1989,1990, 1991). Morphologically a solid tumor has heterogeneous structure, which mainly consists of two discrete regions that are necrotic core and viable zone. Outer region of the tumor surrounded by normal tissue, which includes rapidly divided cells, large blood supply and huge amount of exchange vessels. Inside the tumor, necrosis or mass of premature dead cells is free from functional blood vessels and lymphatic drainage capillaries. On the contrary, within the viable zone, there are functional vessels, which are potentially filtrate blood flow and traverse plasma and therapeutic agent; however, no lymphatic drainage vessels have been reported in the literatures (Baxter and Jain, 1989; Jain et al., 2007). Findings suggest that lack of lymphatic drainage capillaries inside of the tumor may contribute to the elevated IFP, which is believed as a preclusion for efficient drug delivery. Moreover, it is well perceived that tumor can form in various shapes and over growing time, its physiological characteristics can alter. Therefore, current work explores IFP and IFV distributions for different tumor configurations and spatially homogenous and non-homogeneous structures, while surrounding normal tissues are considered. Fig. 1 represents a sample for computational domain of a tumor and its surrounding normal tissue. In scope of the current work, several beneficial assumptions have been made as will be discussed in proceeding.

Comparing the tumor size with order of magnitude O (1 mm) with transcapillary distance inside the interstitium O (1 μm), suggests to deal with the problem macroscopically (Salathe and An, 1976), so that the physiological properties are averaged throughout the tumor and surrounding normal tissue. Additionally, since the time scale of drug transport to the tumor is much less than the tumor growth (Baxter and Jain, 1989), governing equations are simplified to the steady state fashion, as presented in the next section. Finally, it is assumed that tumors undergoes homogeneous perfusion except for the cases at which necrotic core is incorporated in where no functional vasculatures and lymphatic drainage vessels exist.

Governing equations

For the incompressible flow within the interstitium, mass conservation equation incorporating blood extravasation and lymphatic drainage can be modified as:

$$\vec{\nabla} \cdot \left(\gamma \vec{v}\right) = S_m \tag{1}$$

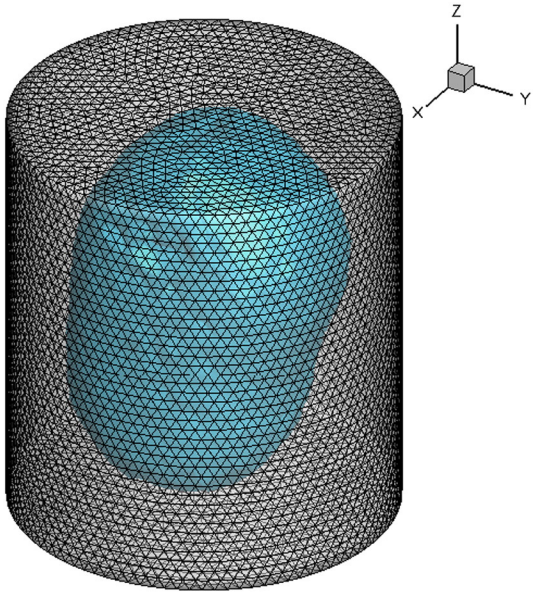

Fig. 1. A sample for computational domain of the tumor and its surrounding normal tissue.

where v is the interstitial fluid velocity (IFV) vector, γ the interstitium porosity and S_m includes effects of fluid exchange between the interstitial space and the blood or lymph vessels. Therefore, S_m can be introduced as:

$$S_m = \frac{J_V}{V} - \frac{J_L}{V} \tag{2}$$

where $\frac{J_V}{V}$ represents the fluid source term (i.e., filtration rate of plasma from blood vessels per unit volume of the tissue) and $\frac{J_L}{V}$ denotes the lymphatic drainage term (i.e., fluid drainage from the interstitial space per unit volume of the tissue). Both terms are included in the continuity equation for the surrounding normal tissue, while inside the tumor, at the viable zone, due to the absence of lymphatic drainage capillaries $\frac{J_L}{V}$ is set to zero. Furthermore, at the necrosis, since there are no filtration and drainage, sink and source terms are eliminated (Baxter and Jain, 1989, 1990). Neglecting inter-capillary blood exchange for vascular blood filtration to the interstitium, source and sink terms from Starling's law (Curry, 1984) are represented as:

$$\frac{J_V}{V} = L_p \frac{S}{V}(p_B - p_i - \sigma(\pi_B - \pi_i)) \tag{3}$$

$$\frac{J_L}{V} = L_{pL} \frac{S_L}{V}(p_i - p_L) \tag{4}$$

where L_p and L_{pL} are the hydraulic conductivities of the microvascular wall and the lymphatic wall, respectively, $\frac{S}{V}$ is the surface area per unit volume for transport to the interstitium, p_B the vascular pressure, p_i the interstitial fluid pressure and p_L denotes the lymphatic hydrostatic pressure. In addition, σ is the average osmotic reflection coefficient for plasma proteins, π_B and π_i are the osmotic pressures of the plasma and the interstitial fluid, respectively. Furthermore, it should be mentioned that in the literatures, the term $p_B - \sigma(\pi_B - \pi_i)$ on the right side of Eq. (3), entitled as effective pressure (p_e) in which, its difference with interstitial pressure determines the amount of fluid filtration inside the interstitium.

For the laminar steady flow through porous media, assuming Newtonian condition and ignoring negligible friction effects inside the interstitium (Baxter and Jain, 1989), the pressure drop would be proportional to the velocity; consequently, the momentum equation can be described by Darcy's law as:

$$\vec{\nabla} p_i = -\frac{\vec{v}}{K} \tag{5}$$

where K is the tissue hydraulic conductivity tensor. In the present work, K is assumed isotropic, so it is reduced to a scalar quantity.

Boundary conditions

In order to obtain a logical estimation of pressure and velocity distributions within the interstitium, appropriate boundary conditions are selected. At the tumor center, assuming no flux, leads to zero pressure gradient equality as follows:

$$\left(\vec{\nabla} p_i\right)_{r=0} = 0 \tag{6}$$

For the distal rim of the normal tissue, zero constant pressure is assumed. However, at the interface of tumor and surrounding normal tissue, continuity condition is invoked for the pressure as follows:

$$K_n \left(\frac{\partial p_i}{\partial n}\right)_{R_t^-} = K_t \left(\frac{\partial p_i}{\partial n}\right)_{R_t^+} \tag{7}$$

$$(p_i)_{R_t^-} = (p_i)_{R_t^+}. \tag{8}$$

Table 1
Baseline properties used in the simulation.

Variable	Tissue	Baseline value
L_p (m Pa^{-1}s^{-1})	Normal	2.7×10^{-12}[a]
	Tumor	2.1×10^{-11}[a]
$\frac{S}{V}$ (m^{-1})	Normal	7000[a]
	Tumor	20000[a]
$\frac{L_{pL} \cdot S_L}{V}$ (Pa^{-1}s^{-1})	Normal	1.042×10^{-6}[a]
P_B (Pa)	Both	2.4×10^{3}[a]
P_L (Pa)	Normal	0[a]
σ	Both	0.82[a]
π_B(Pa)	Both	2.66×10^{3}[a]
π_i(Pa)	Normal	1.33×10^{3}[a]
	Tumor	6.6×10^{2}[a]
K(m^2 Pa^{-1}s^{-1})	Normal	6.39×10^{-15}[a]
	Tumor	3.09×10^{-14}[a]
γ	Normal	0.26[b]
	Tumor	0.3[b]

[a] Baxter and Jain (1989)
[b] J. Zhao et al. (2007).

Physiological properties

In Table 1, employed physiological properties are sorted for tumor and its surrounding normal tissues for parameters, which are appeared in abovementioned equations. These properties are taken from Baxter and Jain (1989) and J. Zhao et al. (2007).

Numerical method

Fluent 6.3 commercial software is employed to solve Eqs. (1)–(5) numerically, while control volume technique is adopted. The source and sink terms in the mass conservation equation for both the tumor and normal tissues are formulated into the main solver rewarding from User Defined Functions (UDFs). In order to find the minimum grid points needed to produce a reasonably grid independent results, extensive computations were performed. It was found that the total number of 179,000 volume cells is required for the grid network. The spatial gradient discretization was achieved by the least squares cell based method. The SIMPLE scheme was used for the pressure–velocity coupling, and the convergence criterion was set to 10^{-10}.

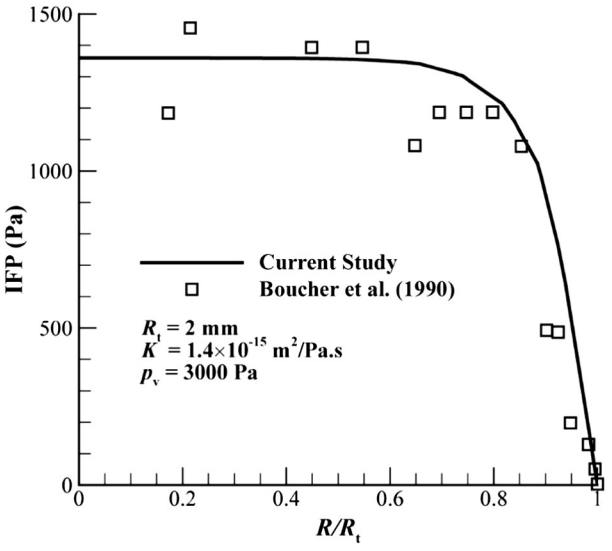

Fig. 2. Comparison of the predicted IFP against the experimental measurements (Boucher et al., 1990) for the mammary adenocarcinoma s.c.

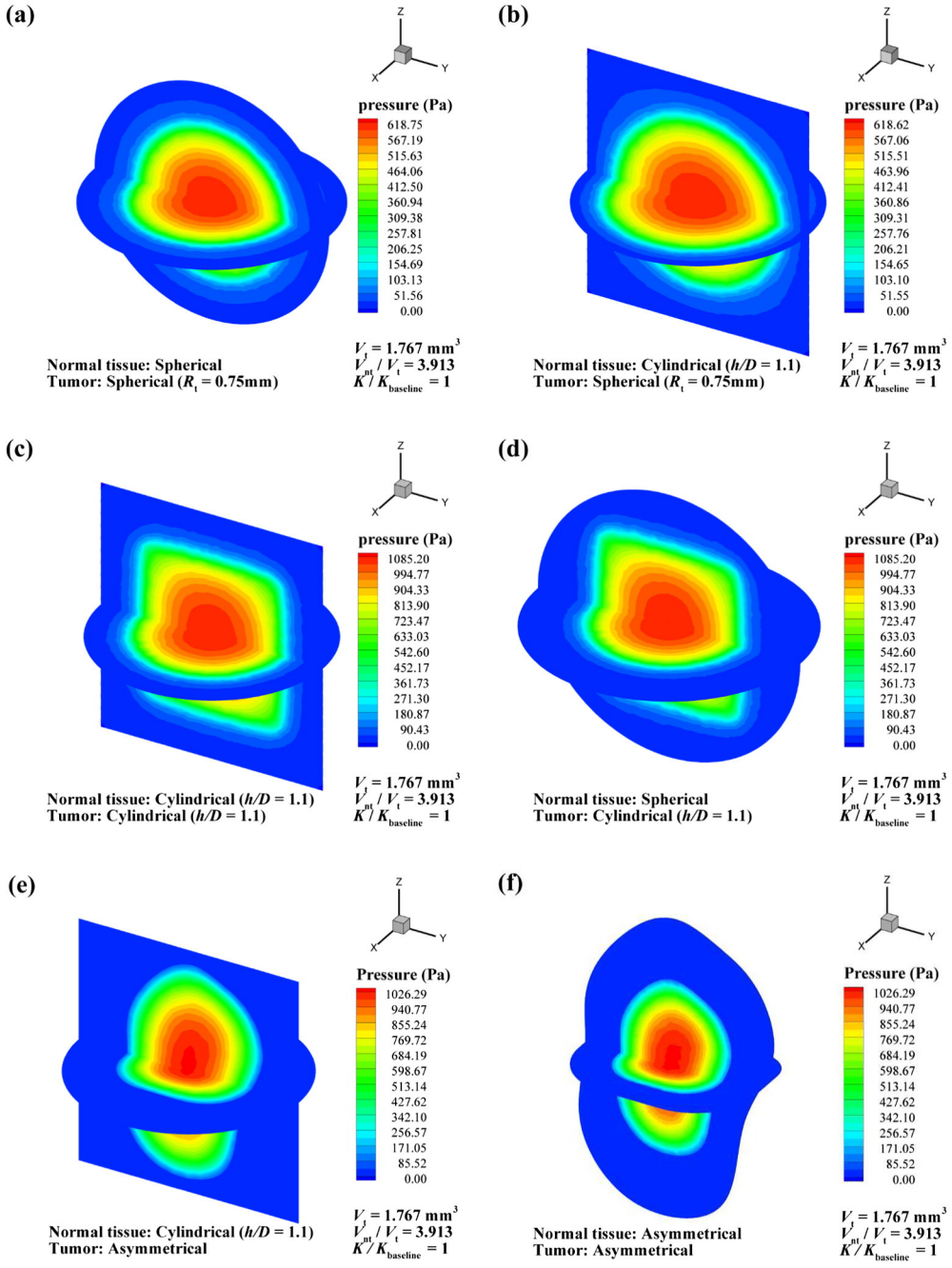

Fig. 3. IFP contours for different configurations of tumors and surrounding normal tissues and $V_t = 1.767$, $V_{nt}/V_t = 3.913$, $K/K_{baseline} = 1$ (a) spherical tumor surrounded by a spherical normal tissue, (b) spherical tumor surrounded by a cylindrical normal tissue, (c) cylindrical tumor surrounded by a cylindrical normal tissue, (d) cylindrical tumor surrounded by a spherical normal tissue, (e) asymmetrical tumor surrounded by a cylindrical normal tissue, and (f) asymmetrical tumor surrounded by an asymmetrical normal tissue.

Results and discussions

In this section, initially, to validate the numerical scheme and its robustness, a comparison has been made by an available experimental data (Boucher et al., 1990). Next, IFP and IFV distributions for various configurations of the tumor and its surrounding normal tissue are compared. Moreover, effects of the tumor radius, normal tissue size and configuration and tissue hydraulic conductivity are examined. Finally, in the last section, incorporating necrotic core inside the tumor, IFP and IFV distributions through a non-homogeneous tumor are explored.

Fig. 2 compares IFP distribution inside the tumor against the experimental measurements by Boucher et al. (1990). As clearly demonstrated, the current result manifests reasonable agreement with the experimental data by just the average deviation of 6.5%.

It is believed that tumors can be formed in different shapes (Soltani and Chen, 2012), as they grow in various organs inside the body. Accordingly, the surrounding normal tissues of the tumors can vary depending on organs they belong. Typically, previous studies assumed surrounding normal tissue alike its tumor, nonetheless in the current paper various configurations of tumor and its surrounding normal tissue are invoked to have an estimation of shape effects on IFP and IFV distributions inside the interstitium. In Fig. 3, contours of IFP are depicted along the horizontal and vertical planes crossing the midpoint of tumors and normal tissues of different shapes. In Figs. 3a and b, tumors are spherical, while the surrounding normal tissues are

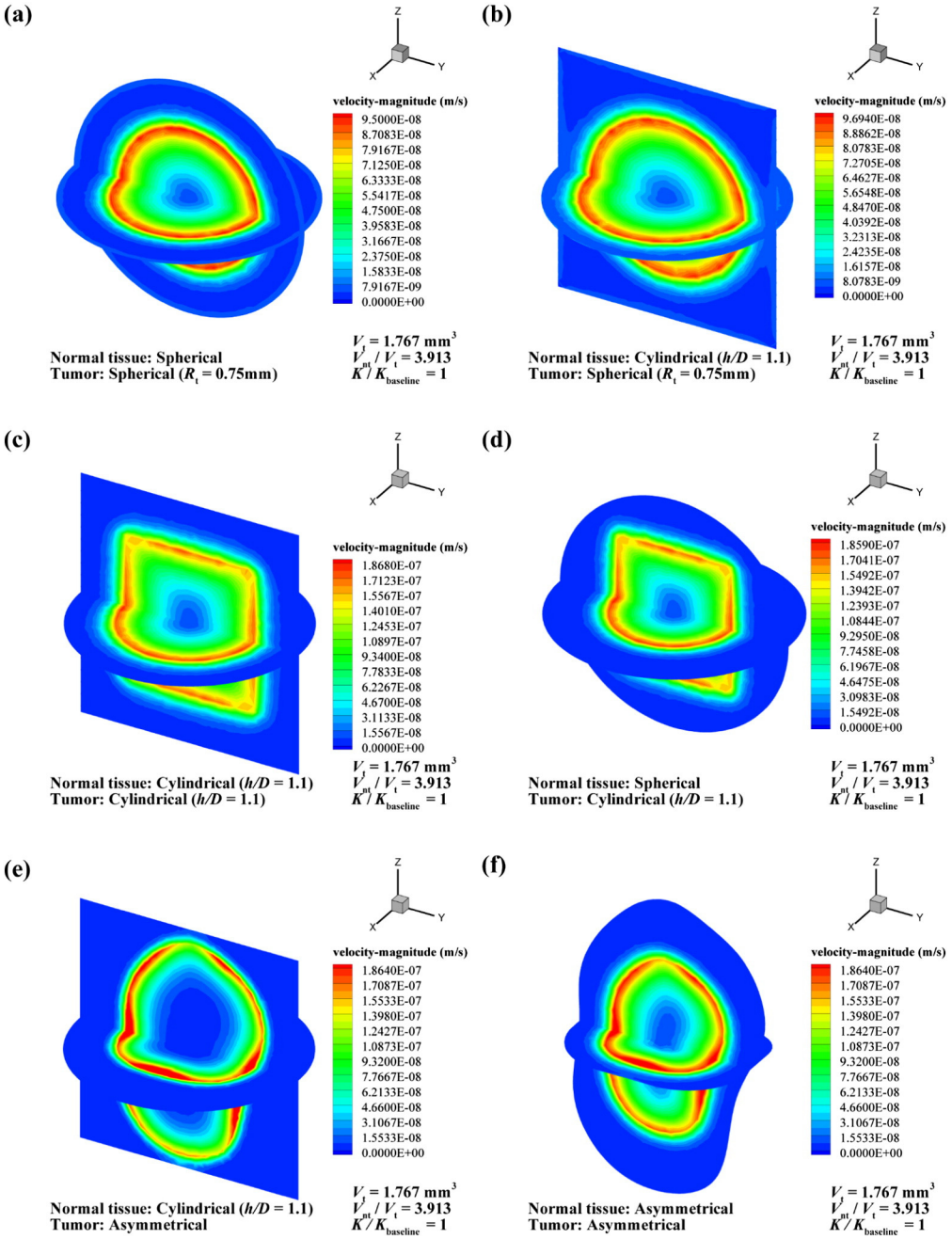

Fig. 4. IFV contours for different configurations of tumors and surrounding normal tissues and $V_t = 1.767$, $V_{nt}/V_t = 3.913$, $K/K_{baseline} = 1$ (a) spherical tumor surrounded by a spherical normal tissue, (b) spherical tumor surrounded by a cylindrical normal tissue, (c) cylindrical tumor surrounded by a cylindrical normal tissue, (d) cylindrical tumor surrounded by a spherical normal tissue, (e) asymmetrical tumor surrounded by a cylindrical normal tissue, and (f) asymmetrical tumor surrounded by an asymmetrical normal tissue.

spherical and cylindrical, respectively. Figs. 3c and d are the same as Figs. 3a and b except for the tumor shape, which is cylindrical. In Figs. 3e and f, the tumors are asymmetrical, while the surrounding normal tissues are cylindrical and asymmetrical, respectively. In these figures, tissues' hydraulic conductivities are held constant and the volumes of the tumors and the normal tissues are chosen to be the same for all configurations, which is equal to 1.767 mm^3 for the tumor and 6.914 mm^3 for the normal tissue. Moreover, the ratio of the normal tissue to the tumor is taken 3.913, based on the value that has been reported by J. Zhao et al. (2007) for a realistic reconstructed model. As shown, generally the IFP increases as it tends to the tumor core and its patterns follow the shape of the tumor itself owing to the assumption of homogenously perfused tumor. Indeed, although the tumor microvasculature is denser and leakier comparing with the surrounding normal tissue, however lack of lymphatic drainage vessels, creates large IFP, which has several impacts on anticancer drug concentration. First, from the Starling law, elevated IFP reduces plasma extravasation inside the tumor, which lowers drug concentration. Second, it reduces the residence time of the therapeutic agents in the tumor interstitium because of fluid convection toward the tumor periphery; the conclusion has been reported by J. Zhao et al. (2007), as well. Finally, as plotted in Fig. 3, emerged convective efflux around the tumor rim blocks fluid infiltration from the normal tissue to the tumor and causes drug heterogeneous concentration.

Moreover, results demonstrate that the IFPs of the cylindrical tumors are higher than that of the spherical ones, which signify the importance of the tumor shape on IFP distribution. Additionally, the IFP value for the irregular shape of tumor (asymmetrical tumor) is closer to that of the

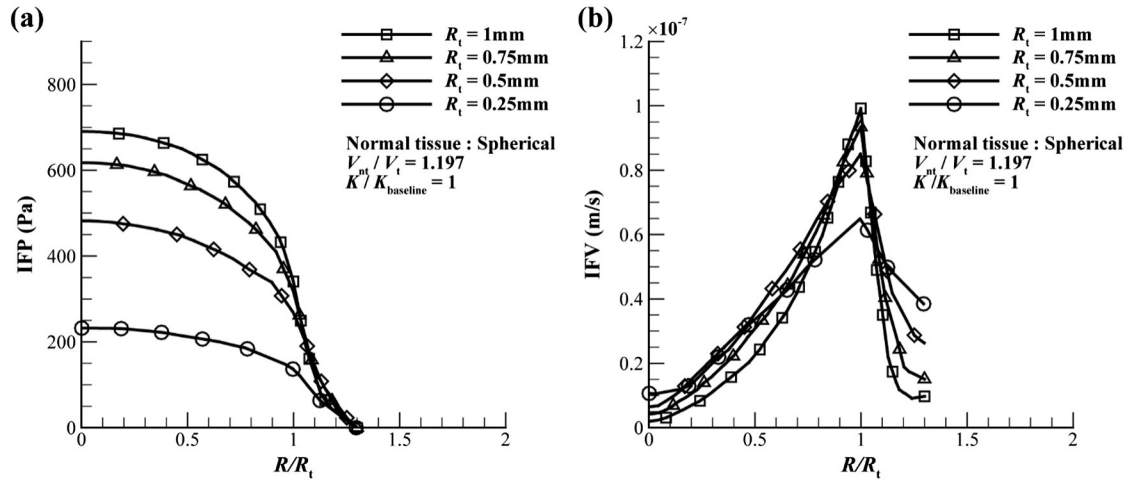

Fig. 5. Radial variations of the a) IFP, b) IFV; for the spherical tumors of different radiuses and surrounded normal tissues with $V_{nt}/V_t = 1.197$ and $K/K_{baseline} = 1$.

cylindrical due to the fact that the geometrical configuration of the asymmetrical tumor is much closer to the cylindrical ones. From the aforementioned description, it can be concluded that as the tumor elongated in the vertical direction, for the same volume, the non-spherical tumor generates higher IFP comparing with the spherical one, the scenario has been occurred for the cylindrical and asymmetrical tumors in Fig. 3. Findings of Soltani and Chen (2012) through extensive numerical exploration on spherical, oblate and prolate tumors were suggested similar upshots. On the contrary, variations of the normal tissue configuration around the tumor impose slight effects on IFP distributions, throughout the tumors and surrounding normal tissues.

Identical to Figs. 3 (a–f) the IFV contours are presented in Figs. 4 (a–f). As clearly depicted, interstitial fluid velocities are approximately in the order of 10^{-7}, which are in good agreements with previous explorations (Jain, 1987; Baxter and Jain, 1989; Jain et al., 2007). Comparing interstitial pressure and velocity contours reveals that the elevated IFPs have contributed to the significant IFVs in the vicinity of the tumors' outer rims and just alike the IFP contours higher IFVs take place for the cylindrical and asymmetrical tumors. Again, it should be noted that various shapes of normal tissue have small effects on IFV distributions.

Fig. 5. displays variations of the IFP and IFV as a function of dimensionless tumor radius for different sizes of the spherical tumors with similar tissue hydraulic conductivities and volume ratios of normal tissue to that of tumor (V_{nt}/V_t). From Fig. 5a, it is clear that the maximum IFP occurs at the tumor core and increases for the larger tumors. Indeed, it can be implied that larger tumors provide more spaces for promoting IFP, meanwhile, by strengthening interstitial resistance against vascular extravasation both from the tumor and surrounding normal tissue, the opportunity for successful drug delivery to the cancer cells decreases remarkably. Again, Fig. 5b clarifies how elevated IFP appears as high IFV at the tumor periphery, which can hinder ample drug influx to the tumor core and resulting heterogeneous drug concentration and unsuccessful treatment. Furthermore, Fig. 5b exhibits that as the tumor becomes smaller, IFV distributes more uniformly inside the normal tissue, while for the larger tumors, IFV drops steeply. Since the volume ratio of the normal tissue to the tumor is held constant, therefore, smaller tumors are surrounded by smaller normal tissue. Consequently, differences in IFV patterns inside the normal tissue can be attributed to its volume variations such that for the larger one, IFV has more space to reach to the lower velocities. Therefore, it can be concluded that for the cases of smaller surrounding normal tissue, larger IFV can be regarded as a barrier against filtrated plasma from the vasculature by removing interstitial fluid from the tumor neighborhood. However, in summary considering Figs. 5a and b collectively, one can infer that tumor therapy through anticancer agents would be more promising if it was accomplished at earlier stages of the formation.

Figs. 6a and b describe effects of the volume size of surrounding normal tissues on IFP and IFV, respectively. In these figures, both the tumors and surrounding normal tissues are assumed spherical. For the case of isolated tumor ($V_{nt}/V_t = 0$), result predicts lower IFP in comparison with the other cases that normal tissues are present; nevertheless for

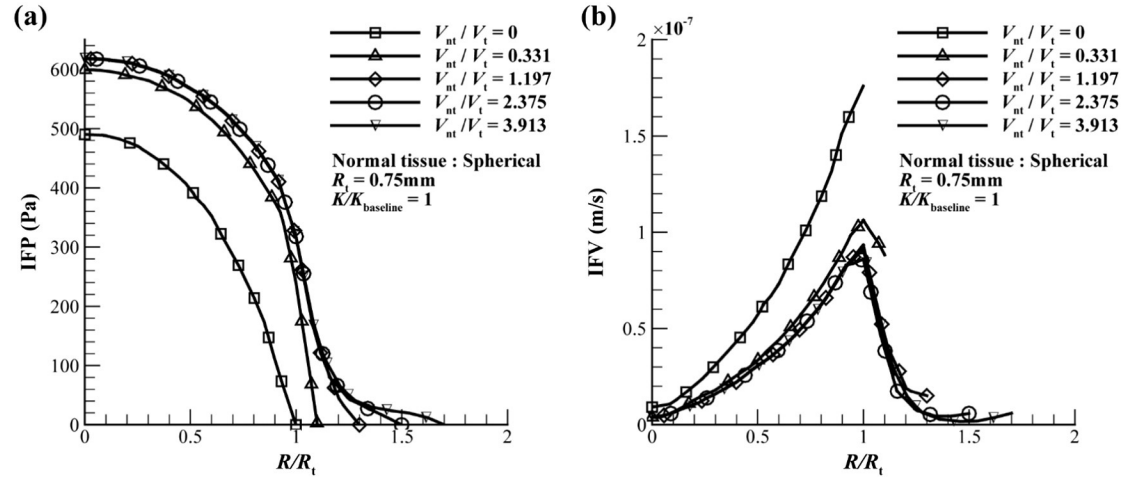

Fig. 6. Radial variations of the a) IFP, b) IFV; for the spherical tumors ($R_t = 0.75$ mm) which is surrounded by different volumes of spherical normal tissues and $K/K_{baseline} = 1$.

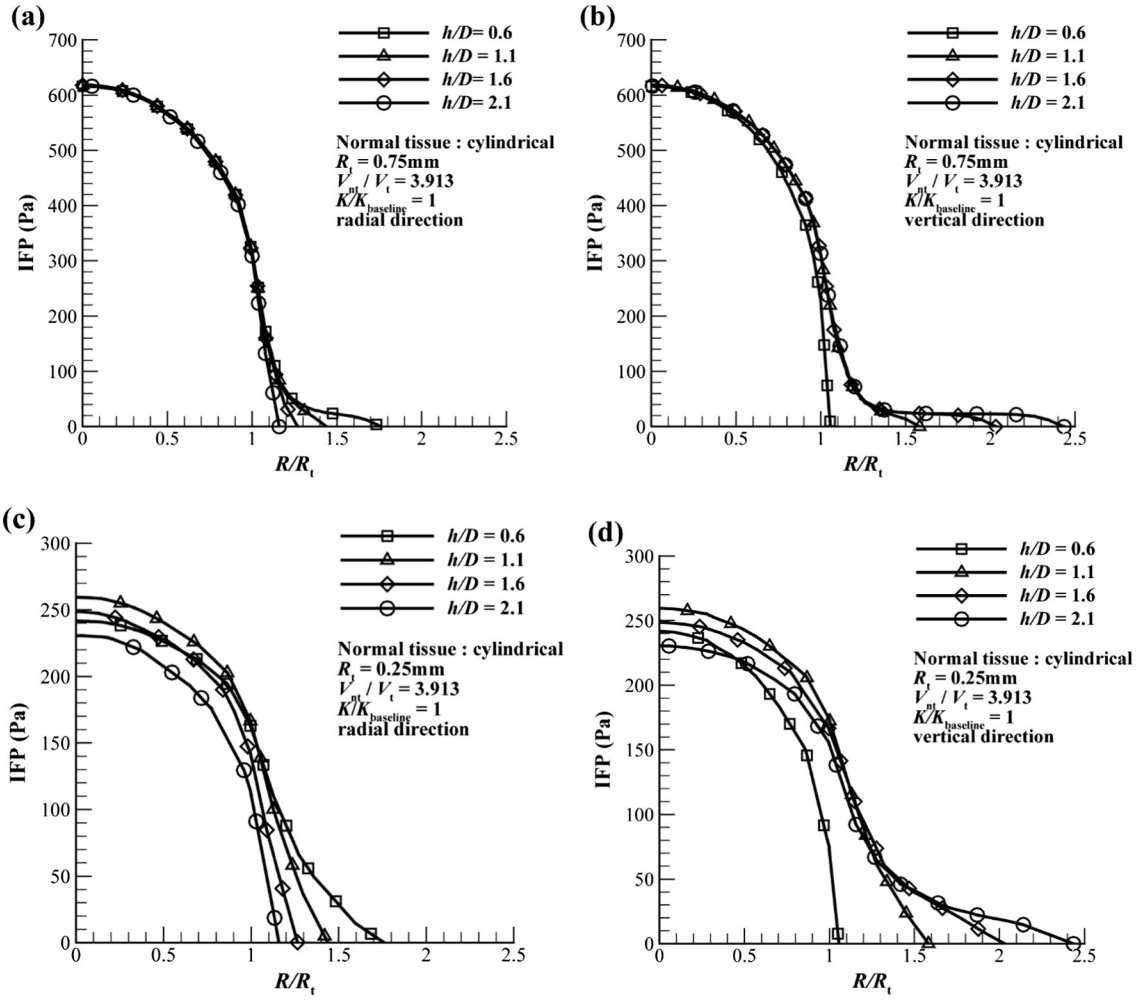

Fig. 7. Radial variations of the IFP for a) $R_t = 0.75$ mm, in the radial direction; b) $R_t = 0.75$ mm, in the vertical direction; c) $R_t = 0.25$ mm, in the radial direction; d) $R_t = 0.25$ mm, in the vertical direction; for different values of (h/d) of the cylindrical normal tissue and $V_{nt}/V_t = 3.913$, $K/K_{baseline} = 1$.

the isolated case IFV always experiences ascending pattern, which reaches to the maximal at the tumor outer rim. Moreover, current study estimates IFV at the tumor periphery around 0.17 μm for the isolated tumor that shows good agreement with experimental measurement of Butler et al. (1975) and analytical solution of Baxter and Jain (1989). On the other hand, for the cases with surrounding normal tissues, IFPs increase and approach to zero value at distal regions of the tumor core in the normal tissue interstitium, while IFVs reduce, which can address to the existence of surrounding normal tissues. Finally, it is noteworthy to mention that for the cases of $(V_{nt}/V_t) > 1$ nearly slight variations can be observed for both IFP and IFV; and normal tissue size effect seems to be negligible.

In the previous part, effects of the different volume ratio of the normal tissue to the tumor are examined. In this part for a constant volume ratio of 3.913 and spherical tumors with the radiuses of 0.75 mm and 0.25 mm, effects of normal tissue elongation are studied. To this aim, the ratio of cylinder height to its radius for the cylindrical normal tissue is varied and the variation effects are studied. Figs. 7 (a,b) and 8 (a,b) display IFPs and IFVs, respectively, for various ratios of (h/d) of the cylindrical normal tissue and 0.75 mm tumor radii in radial and vertical directions, while Figs. 7(c,d) and 8(c,d) describe similar scenarios for the 0.25 mm tumor radii. Based on the previous discussion on tumor size, IFP variations are more pronounced for larger tumor; moreover, Figs. 7 (a,b) show that for the tumor radius of 0.75 mm no deviations can be observed in IFP at the tumor core. While, Figs. 7(c,d) for the tumor radius of 0.25 mm, suggest slight variations in maximum IFPs at the tumor core. More interestingly, comparing variation trends of IFPs reveals that along the vertical direction, as the normal tissue is more elongated, IFPs show much variations comparing with the radial direction and zero IFPs take place in farther regions. Similarly, higher IFVs are resulted for the larger tumors and their variations are more pronounced in the vertical direction.

Generally, for the assumed cylindrical surrounding normal tissues, the severity of variations is more dramatic along the tumor heights. Besides, for the faces of the tumor in which there are more space of surrounding normal tissue, IFP drops more moderately through the interstitium and convective velocity especially at the outer rim of the tumor reduces, which can enhance the efficiency of drug delivery to the tumor from those sites.

The sensitivity of the tumor to the hydraulic conductivity of the interstitium is examined for the spherical tumor and its surrounding normal tissue in Fig. 9. Generally, increasing hydraulic conductivities of the tumor and normal tissue interstitium lowers IFP, which can lead to the higher concentration of therapeutic agents inside the tissue. Indeed, based on Starling's law for the vasculature extravasation, by increasing the difference between IFP and effective pressure, rate of the filtrated flow from the vasculature to the interstitium increases. Furthermore, for the higher hydraulic conductivities, IFVs inside the tumors decrease and facilitate drug delivery through cancerous tissues.

In the last section, effects of the heterogeneous structure of the tumor are investigated, considering necrosis and the viable zone, simultaneously. For a spherical tumor with 0.75 mm radius that is surrounded

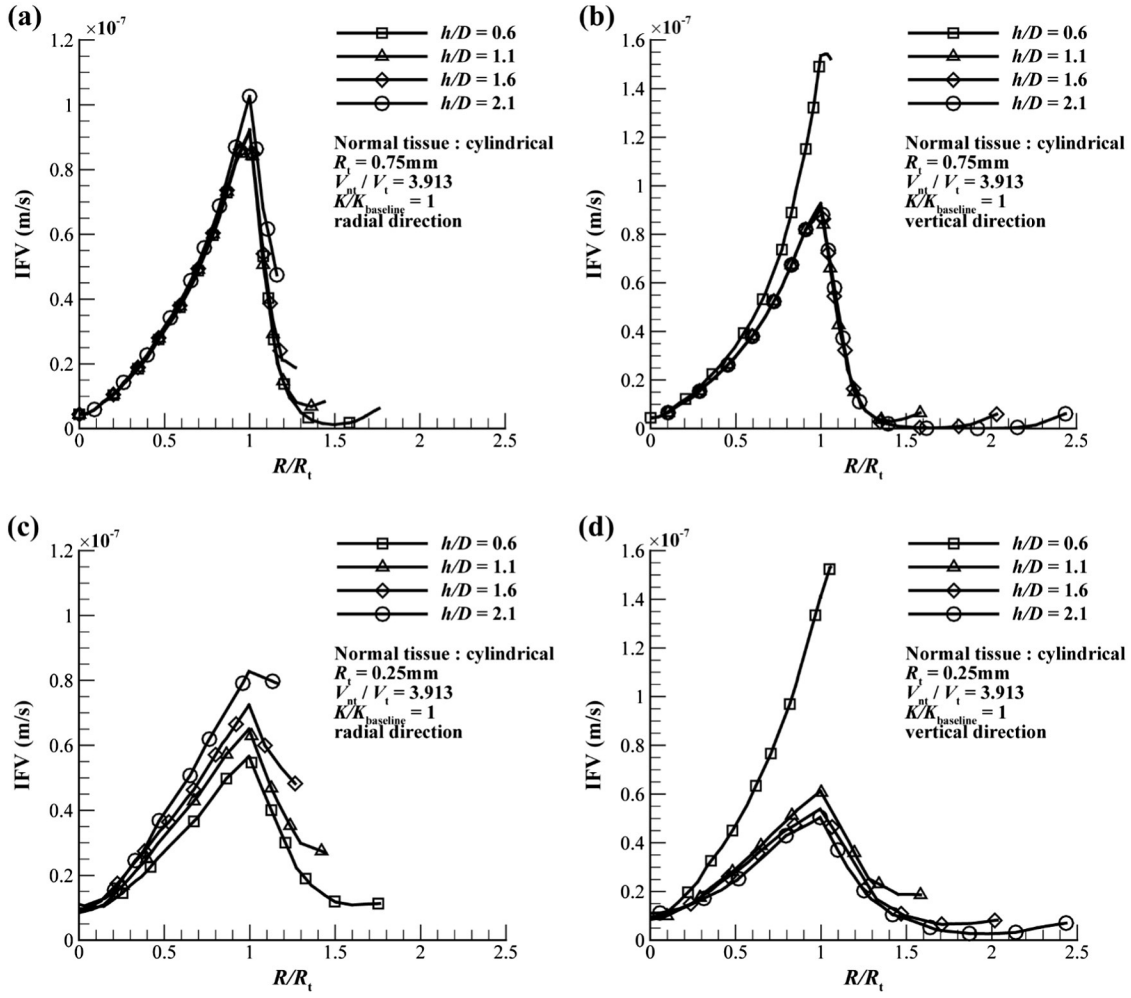

Fig. 8. Radial variations of the IFV for a) $R_t = 0.75$ mm, in the radial direction; b) $R_t = 0.75$ mm, in the vertical direction; c) $R_t = 0.25$ mm, in the radial direction; d) $R_t = 0.25$ mm, in the vertical direction; for different values of (h/d) of the cylindrical normal tissue and $V_{nt}/V_t = 3.913$, $K/K_{baseline} = 1$.

by a spherical normal tissue, a necrosis with the radius of 5 times smaller than the tumor is assumed. Also in order to investigate effects of the necrosis location on IFP and IFV, the simulation has been carried out for five location of the necrosis along y-axis. Figs. 10a and b demonstrate IFPs and IFVs for different locations of the necrotic core, respectively. Additionally, to have a wider view of the IFV distribution in the heterogeneous tumor Fig. 10c is plotted across y–z plane for the various positions of the necrosis. Recalling from previous section, necrosis is a mass of dead cells in the tumor, where no fluid extravasation and drainage exist due to the lack of filtration vasculature and lymphatic vessels. Considering Fig. 10a, IFPs vary in conventional mode, i.e., a maximum in the tumor core, and gradual reduction as moving toward the normal

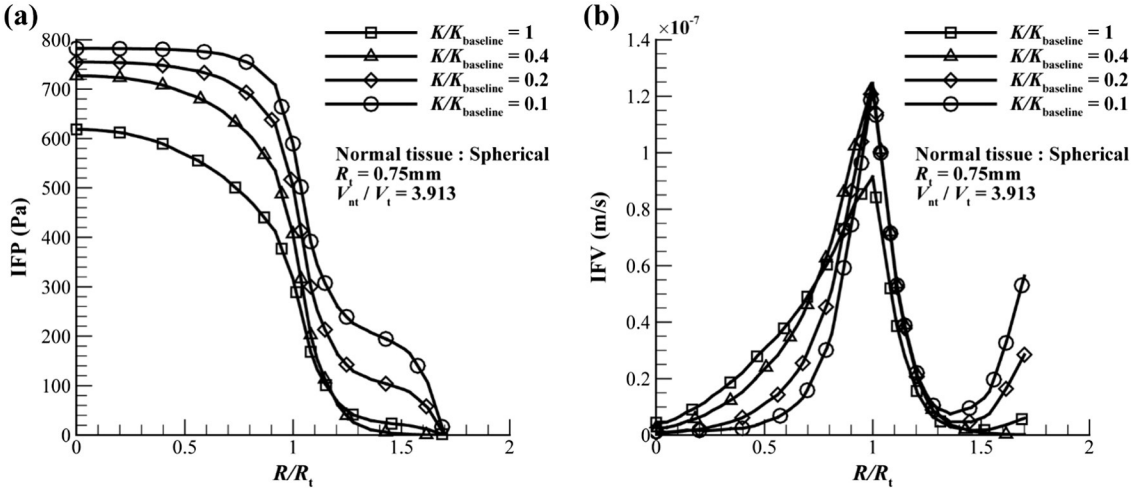

Fig. 9. Radial variations of the a) IFP, b) IFV; for the spherical tumors ($R_t = 0.75$ mm) with different tissue hydraulic conductivities surrounded by spherical normal tissues and $V_{nt}/V_t = 3.913$.

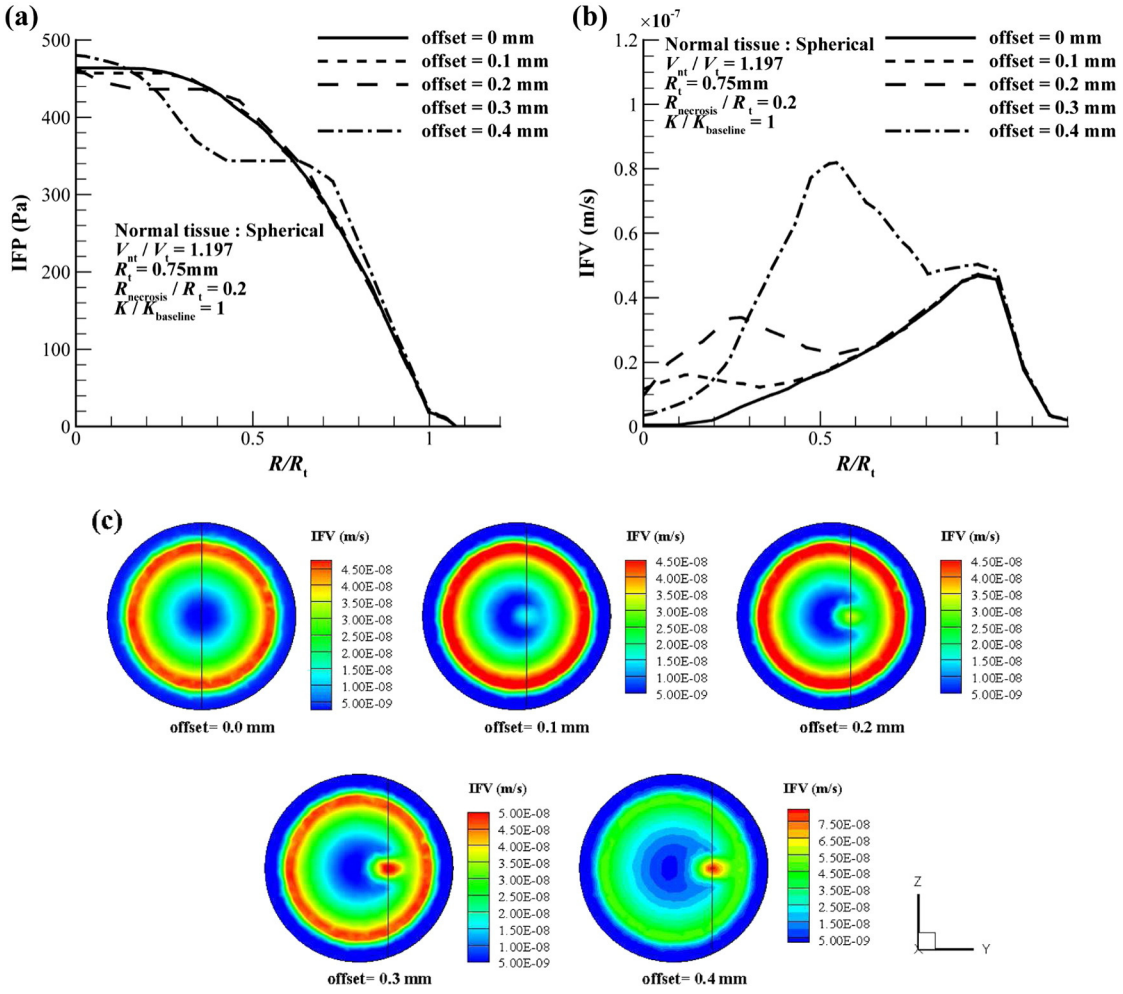

Fig. 10. Radial variations of the (a) IFP, (b) IFV; for the spherical tumors ($R_t = 0.75$ mm) including necrosis and surrounding normal tissue, and $V_{nt}/V_t = 1.197$, $R_{necrosis}/R_t = 1$, $K/K_{baseline} = 1$ (c) IFV contours on y–z plane.

tissue, however, as clearly displayed, across the necrosis, IFPs remain constant. The interesting point is the appearance of IFV local maximum approximately at the center of necrosis such that by moving toward the tumor outer rim, its value raises. Therefore, the most important point that can be implied is that at the necrosis the local increase in IFV can hinder proper plasma filtration, especially at its neighborhood, where still living cancer cells exist, which consequently lead to the poor drug delivery.

Conclusion

In this study, one of the crucial mechanisms, which affect drug delivery to the cancerous tissues, is investigated. The interstitial fluid transport of the tumor and its surrounding normal tissue is simulated using the porous media model. Darcy's law for the fluid motion inside the porous mediums along with the continuity equation is solved numerically. For employing extravascular filtration of blood and lymphatic drainage vessels continuity equation is modified by employing Starling's Law. The predicted results agree well with the available experimental measurements in the literature. Results indicate that tumor size has considerable effects on IFP and IFV distributions such that by increasing tumor size both IFP and IFV raise and block drug infiltration to the tumor via convection. In contrast, examining various shapes and volumes of surrounding normal tissue shows moderate effect on IFP and IFV inside the tumor and its surrounding normal tissue, except for the isolated tumor that suggests remarkable changes. Moreover, findings predict that higher hydraulic conductivity of the interstitium lowers IFP inside the tumor and IFV at tumor rim. Therefore, employing proper therapeutic methods, which can enhance hydraulic conductivity of the interstitium, would promote drug delivery. Finally, necrosis inside the tumor reveals significant effects on IFV and IFP, especially as distance from the tumor core IFV increases dramatically. Thus, it can be concluded that necrosis and its location could alter IFP and IFV and more crucially the effectiveness of drug delivery to the tumor interstitium.

Conflict of interest statement

There are no financial and personal relationships with other people or organizations that could inappropriately influence (bias) their work.

References

Anderson, A.R., Chaplain, M., 1998. Continuous and discrete mathematical models of tumor-induced angiogenesis. Bull. Math. Biol. 60, 857–899.
Baxter, L.T., Jain, R.K., 1989. Transport of fluid and macromolecules in tumors. I. Role of interstitial pressure and convection. Microvasc. Res. 37, 77–104.
Baxter, L.T., Jain, R.K., 1990. Transport of fluid and macromolecules in tumors. II. Role of heterogeneous perfusion and lymphatics. Microvasc. Res. 40, 246–263.
Baxter, L.T., Jain, R.K., 1991. Transport of fluid and macromolecules in tumors: III. Role of binding and metabolism. Microvasc. Res. 41, 5–23.
Boucher, Y., et al., 1990. Interstitial pressure gradients in tissue-isolated and subcutaneous tumors: implications for therapy. Cancer Res. 50, 4478–4484.
Butler, T.P., et al., 1975. Bulk transfer of fluid in the interstitial compartment of mammary tumors. Cancer Res. 35, 3084–3088.
Cai, Y., et al., 2011. Coupled modelling of tumour angiogenesis, tumour growth and blood perfusion. J. Theor. Biol. 279, 90–101.

Curry, F., 1984. Mechanics and thermodynamics of transcapillary exchange. Handb. Physiol. 4, 309–374.
El-Kareh, A.W., Secomb, T.W., 1995. Effect of increasing vascular hydraulic conductivity on delivery of macromolecular drugs to tumor cells. Int. J. Radiat. Oncol. Biol. Phys. 32, 1419–1423.
Goh, Y.-M.F., et al., 2001. Simulation of the delivery of doxorubicin to hepatoma. Pharm. Res. 18, 761–770.
Harrington, H.A., et al., 2007. A hybrid model for tumor-induced angiogenesis in the cornea in the presence of inhibitors. Math. Comput. Model. 46, 513–524.
Jain, R.K., 1987. Transport of molecules in the tumor interstitium: a review. Cancer Res. 47, 3039–3051.
Jain, R.K., 1988. Determinants of tumor blood flow: a review. Cancer Res. 48, 2641–2658.
Jain, R.K., 2005. Normalization of tumor vasculature: an emerging concept in antiangiogenic therapy. Science 307, 58–62.
Jain, R.K., Baxter, L.T., 1988. Mechanisms of heterogeneous distribution of monoclonal antibodies and other macromolecules in tumors: significance of elevated interstitial pressure. Cancer Res. 48, 7022–7032.
Jain, R.K., et al., 2007. Effect of vascular normalization by antiangiogenic therapy on interstitial hypertension, peritumor edema, and lymphatic metastasis: insights from a mathematical model. Cancer Res. 67, 2729–2735.
Linninger, A.A., et al., 2008. Computational methods for predicting drug transport in anisotropic and heterogeneous brain tissue. J. Biomech. 41, 2176–2187.
Netti, P.A., et al., 1995. Time-dependent behavior of interstitial fluid pressure in solid tumors: implications for drug delivery. Cancer Res. 55, 5451–5458.
Pishko, G.L., et al., 2011. Sensitivity analysis of an image-based solid tumor computational model with heterogeneous vasculature and porosity. Ann. Biomed. Eng. 39, 2360–2373.
Pozrikidis, C., Farrow, D.A., 2003. A model of fluid flow in solid tumors. Ann. Biomed. Eng. 31, 181–194.
Salathe, E.P., An, K.-N., 1976. A mathematical analysis of fluid movement across capillary walls. Microvasc. Res. 11, 1–23.
Sefidgar, M., et al., 2014. Effect of tumor shape, size, and tissue transport properties on drug delivery to solid tumors. J. Biol. Eng. 8, 12.
Sefidgar, M., et al., 2015. Numerical modeling of drug delivery in a dynamic solid tumor microvasculature. Microvasc. Res.
Siegel, R., et al., 2013. Cancer statistics, 2013. CA Cancer J. Clin. 63, 11–30.
Soltani, M., Chen, P., 2011. Numerical modeling of fluid flow in solid tumors. PLoS ONE 6, e20344.
Soltani, M., Chen, P., 2012. Effect of tumor shape and size on drug delivery to solid tumors. J. Biol. Eng. 6.
Soltani, M., Chen, P., 2013. Numerical modeling of interstitial fluid flow coupled with blood flow through a remodeled solid tumor microvascular network. PLoS ONE 8, e67025.
Stéphanou, A., et al., 2006. Mathematical modelling of the influence of blood rheological properties upon adaptative tumour-induced angiogenesis. Math. Comput. Model. 44, 96–123.
Tan, W.H., et al., 2003. Computer simulation of the delivery of etanidazole to brain tumor from PLGA wafers: comparison between linear and double burst release systems. Biotechnol. Bioeng. 82, 278–288.
Teo, C.S., et al., 2005. Transient interstitial fluid flow in brain tumors: effect on drug delivery. Chem. Eng. Sci. 60, 4803–4821.
Wang, C.-H., Li, J., 1998. Three-dimensional simulation of IgG delivery to tumors. Chem. Eng. Sci. 53, 3579–3600.
Wang, C.-H., et al., 1999. The delivery of BCNU to brain tumors. J. Control. Release 61, 21–41.
Yifat, J., Gannot, I., 2014. 3D discrete angiogenesis dynamic model and stochastic simulation for the assessment of blood perfusion coefficient and impact on heat transfer between nanoparticles and malignant tumors. Microvasc. Res. 98, 197–217.
Zhao, G., et al., 2007a. Numerical simulation of blood flow and interstitial fluid pressure in solid tumor microcirculation based on tumor-induced angiogenesis. Acta Mech. Sinica 23, 477–483.
Zhao, J., et al., 2007b. Effect of heterogeneous vasculature on interstitial transport within a solid tumor. Microvasc. Res. 73, 224–236.